ADVANCED ENERGY MATERIALS
www.advenergymat.de

Materials Views
www.MaterialsViews.com

Strong Visible-Light Absorption and Hot-Carrier Injection in $TiO_2/SrRuO_3$ Heterostructures

*Sungki Lee, Brent A. Apgar, and Lane W. Martin**

Correlated electron oxides prove a diverse landscape of exotic materials' phenomena and properties. One example of such a correlated oxide material is strontium ruthenate ($SrRuO_3$) which is known to be a metallic itinerant ferromagnet and for its widespread utility as a conducting electrode in oxide heterostructures. We observe that the complex electronic structure of $SrRuO_3$ is also responsible for unexpected optical properties including high absorption across the visible spectrum (commensurate with a low band gap semiconductor) and remarkably low reflection compared to traditional metals. By coupling this material to a wide band gap semiconductor (TiO_2) we demonstrate dramatically enhanced visible light absorption and large photocatalytic activities. The devices function by photo-excited hot-carrier injection from the $SrRuO_3$ to the TiO_2 and the effect is enhanced in thin films due to electronic structure changes. This observation provides an exciting new approach to the challenge of designing visible-light photosensitive materials.

1. Introduction

The primary feature limiting the performance of oxide-based photovoltaic and/or photocatalytic systems has traditionally been the poor absorption of visible light in these often wide band gap materials. One candidate oxide material for such applications is anatase TiO_2 which is arguably the most widely-studied photocatalyst[1,2] (due to its chemical stability, non-toxicity, low-cost, and excellent band alignment to several oxidation-reduction reactions) and serves as the backbone of dye-sensitized solar cells[3,4] where the presence of a light-absorbing dye accounts for the critical flaw of TiO_2: a large band gap (3.2-3.6 eV) which limits efficient usage of all but the UV portion of sunlight. When designing next generation solar energy conversion systems (i.e., photovoltaics, photocatalysis, etc.) the goal is clear: develop a way to more efficiently utilize the solar spectrum. To address this material deficiency, research has focused on two major approaches: 1) chemical modifications to tune the band gap of TiO_2 and 2) synthesis of composite heterojunctions that combine strong light absorbing materials with the catalytic activity of TiO_2.

In this spirit, considerable effort has focused on doping or alloying TiO_2 to change the band gap. This work falls into two main categories: 1) metal or 2) non-metal doping. Metal-doping is believed to generate new energy levels (i.e., defect states) within the band gap and it is thought that transition metal doping can also improve the trapping of electrons to inhibit electron-hole recombination during irradiation but generally results in degraded charge carrier lifetimes.[5] Non-metal doping is thought to impact the band structure in one of a number of possible ways,[6] but the most effective has been through band gap narrowing as was observed in N-doped TiO_2 where the band gap can be narrowed by ~0.72 eV as a result of the N 2*p* states hybridizing with the O 2*p* states.[7] Regardless of the mechanism at play, these approaches have been demonstrated to be only minimally effective at impacting the electronic structure and properties. At the same time, much work has explored the concept of what has generically been called photochemical diodes.[8] By combining TiO_2 with another semiconductor (i.e., one that might promote additional light absorption or more efficient charge separation) the overall performance can be improved. This includes combining TiO_2 with small band gap semiconductors such as CdS[9] and other oxide semiconductors such as SnO_2[10] and ZnO.[11] For a more complete review of various geometries, materials, and architectures in this realm see Ref. [12].

More recently, considerable attention has been given to a topic called hot-carrier injection.[13,14] Hot-carrier injection has been demonstrated to be important for photovoltaics because it could provide a way to overcome limits to theoretical efficiencies in traditional semiconductor devices by utilizing high-energy, photo-excited carriers with very short lifetimes instead of relying on minority carrier transport. Recently hot-carrier injection was observed in quantum-dot-PbSe/Rutile-TiO_2 wherein injection was attributed to the slow electronic relaxation in the PbSe and accepting surface states on the TiO_2 thereby avoiding losses resulting from the thermalization of photo-excited carriers.[15,16] The role of hot-carrier injection has also been explored in the context of photocatalysis.[17,18]

In this manuscript, we explore a new manifestation of a TiO_2-based composite heterojunction designed to promote

S. Lee, B. A. Apgar, Prof. L. W. Martin
Department of Materials Science and Engineering
and Materials Research Laboratory,
University of Illinois, Urbana-Champaign
Urbana, IL 61801, USA
International Institute for Carbon Neutral Energy Research
744 Motooka, Nishi-ku, Fukuoka 819-0395, Japan
E-mail: lwmartin@illinois.edu

DOI: 10.1002/aenm.201201116

more efficient utilization of the solar spectrum for energy applications. We report on photovoltaic and photocatalytic effects in heterojunctions of anatase TiO_2 together with a strongly absorbing "metallic" oxide $SrRuO_3$ that has structural, electronic, and chemical compatibility with TiO_2. $SrRuO_3$ is a correlated electron oxide which is known to possess metal-like temperature dependence of its resistivity and itinerant ferromagnetism and for its widespread utility as a conducting electrode in oxide heterostructures.[19] Referring to this material as a "metal," however, is likely inappropriate as the electronic structure and properties are derived from a combination of complex electronic density of states, electron correlations, and more. We observe that the unusual electronic structure of $SrRuO_3$ is also responsible for unexpected optical properties including high absorption across the visible spectrum and low reflection compared to traditional metals. By coupling this material to TiO_2 we demonstrate enhanced visible light absorption and large photocatalytic activities. The devices function by photo-excited hot-carrier injection from the $SrRuO_3$ to the TiO_2. This observation provides an exciting new approach to the challenge of designing visible-light photosensitive materials.

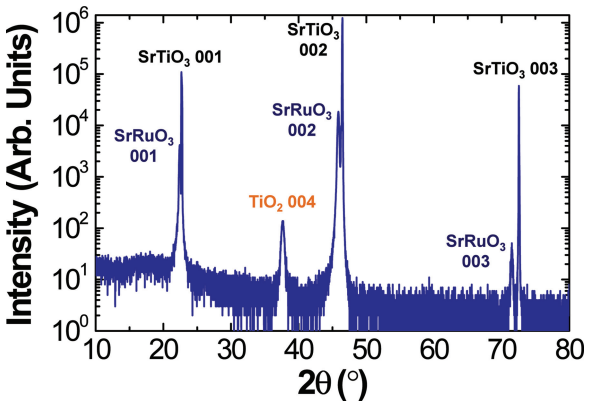

Figure 1. θ-2θ X-ray diffraction study of a 25 nm TiO_2/ 50 nm $SrRuO_3$/ $SrTiO_3$ (001) heterostructure.

2. Results and Discussion

2.1 Structural and Optical Properties

Epitaxial thin film versions of the materials of interest were grown via pulsed-laser deposition (details of which are provided in the Experimental Section). For this work, $SrRuO_3$ thin films were varied from 5-100 nm, anatase TiO_2 films were varied from 10-100 nm, and all films were grown on $SrTiO_3$ (001) substrates. The structure, phase, and orientations of the films were characterized by X-ray diffraction. A typical diffraction pattern for a 25 nm TiO_2/50 nm $SrRuO_3$/$SrTiO_3$ (001) heterostructure shows that the films are single phase, 00*l* oriented, and that the TiO_2 forms in the anatase structure (**Figure 1**). Following growth and structural characterization, we proceeded to study the optical properties of the $SrRuO_3$ thin films. The optical properties were characterized by photospectrometry (to probe UV-Visible-near-IR transmittance, reflectance, and absorbance) and variable-angle spectroscopic ellipsometry (to probe refractive index, *n*, and extinction coefficient, *k*). The reflectance of a 50 nm $SrRuO_3$/$SrTiO_3$ (001) heterostructure, as measured by photospectrometry and calculated from *n* and *k* (Supporting Information, Figure S1a, b), was found to be 20-25% across the entire range of visible light (**Figure 2**a). As a comparison, the values of reflectance for representative elemental metals Al, Au, Pt, and Ti[20,21] are generally in excess of 80-90% across the same range of wavelengths. The discrepancy between the low reflectance in the $SrRuO_3$ and the elemental metals indicates that the electronic structure of the former gives rise to dramatically different optical properties. Additionally, the absorption coefficient (α) (calculated from transmission and reflection data (Supporting Information, Figure S1c, d) and from *k*) is found to peak at ~320 nm and shows high values (in excess of 1.5×10^5 cm^{-1}) across the entire visible light range (Figure 2b). For comparison, the absorption coefficient for the widely used semiconductor silicon is approximately 1-to-3 orders-of-magnitude smaller than that of $SrRuO_3$ across this same range of wavelengths. Furthermore, the absorbance of the $SrRuO_3$ films is observed to increase with increasing film thickness

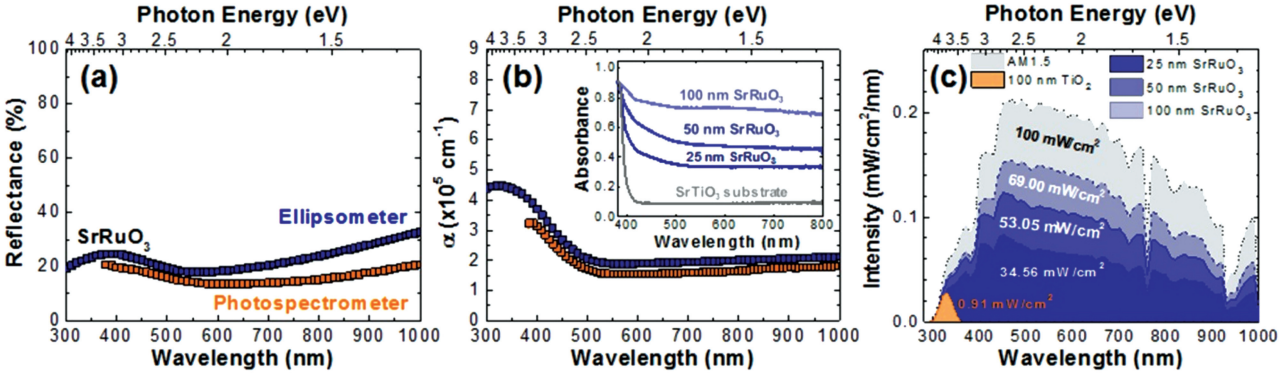

Figure 2. (a) Reflectance and (b) absorption coefficient (α) of a 50 nm $SrRuO_3$/$SrTiO_3$ (001) heterostructure as measured via photospectrometry (orange) and ellipsometry (blue). The inset of (b) shows the absorbance from 25, 50, and 100 nm thick $SrRuO_3$/$SrTiO_3$ (001) heterostructures. (c) Absorption spectrum of 100 nm TiO_2 and 25, 50, and 100 nm $SrRuO_3$ films overlaid on the AM1.5G spectrum.

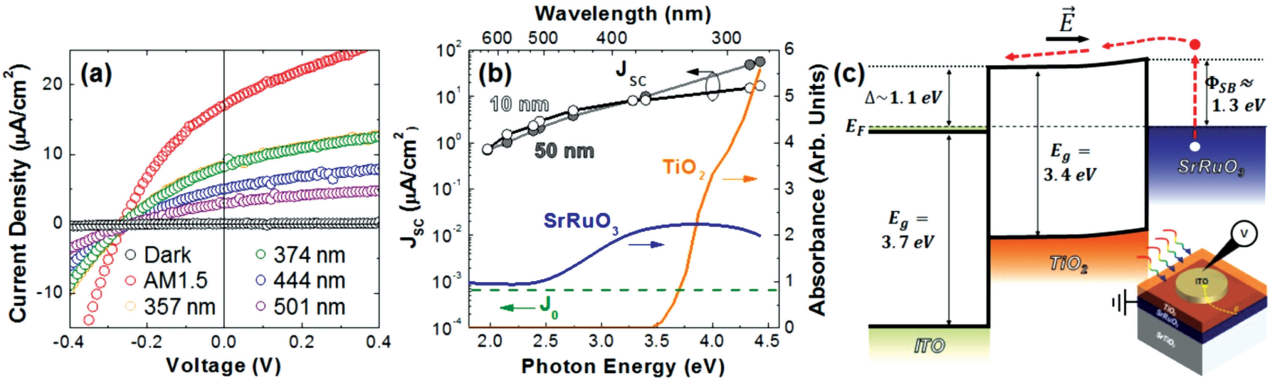

Figure 3. (a) Light and dark current-voltage characteristics of a 100 nm ITO/ 100 nm TiO_2/ 10 nm $SrRuO_3$ device taken with different longpass glass filters (the number in the key represents the λ_{OD2} of the filter). (b) Short-circuit current density (J_{SC}) as a function of photon energy for devices with 10 and 50 nm of $SrRuO_3$ measured under AM1.5G illumination with various longpass glass filters as compared to the dark diode current through the device (J_0) and the absorbance of the $SrRuO_3$ and TiO_2 films. (c) Schematic band diagram of hot-carrier injection in the ITO/ TiO_2/ $SrRuO_3$ Schottky junction device.

and matches the trend expected from the Beer-Lambert law (Figure 2b, inset).

The implication of this absorption for solar energy applications is illustrated by comparing the fraction of the AM1.5G light spectrum that is absorbed by $SrRuO_3$ and TiO_2 (Figure 2c). The absorption spectra are calculated from the experimentally measured reflectance and absorption coefficient which allows us to calculate the non-reflected light spectrum (I_1) from the reference AM1.5G spectrum (I_0) (as obtained from the ASTM G-173-03 Reference Spectra) as $I_1 = I_0(1 - R)$. This gives a measure of the non-reflected light that enters of the $SrRuO_3$ layer. Then, using the Beer-Lambert law we can obtain the transmitted light intensity $I_2 = I_1\, e^{-\alpha t}$ where t is thickness of the $SrRuO_3$ film. Finally, the absorbed light spectra are obtained by subtracting I_2 from I_1. From such an analysis, we find that a 100 nm TiO_2 thin film absorbs only 0.91 mW/cm^2 of the 100 mW/cm^2 AM1.5G spectrum (orange area, Figure 2c) while a 100 nm $SrRuO_3$ thin film absorbs a remarkable 69 mW/cm^2 (Figure 2c). These results indicate that $SrRuO_3$, despite exhibiting the electronic character of a *bad* metal (decreasing resistivity with decreasing temperature),[22,23] behaves optically as a semiconductor. Again, for comparison, a 100 nm thick film of silicon would absorb only 6.9 mW/cm^2–an order of magnitude less than $SrRuO_3$ of the same thickness. Additionally, although $SrRuO_3$ has been widely studied in the condensed matter physics community and is utilized as a metal oxide electrode for the epitaxial growth of many functional oxide thin-film devices[19] the use of this material as an optical absorber for photosensitive devices has not been considered.

This strong light absorption is supported by experimental[24–26] and first-principle[27,28] studies of the electronic structure. In $SrRuO_3$ there is a high electronic density-of-states (DOS) at the Fermi energy (E_F) associated with a quasiparticle band and occupied and unoccupied portions of the split Ru t_{2g} bands. This structure, which has been explained using dynamic mean field theory,[29] arises because $SrRuO_3$ exists near a Mott transition and thus its one-particle spectral function will be split into two Hubbard bands in addition to the quasiparticle band located at the E_F. Additionally, the upper Hubbard band may further split into states of t_{2g} and e_g symmetry. For $SrRuO_3$, electron-electron correlations are quite weak and the Hubbard bands merge to form a single partly filled band at E_F.[26] The result is that in $SrRuO_3$ there is essentially a continuous DOS above E_F which allows for optical inter- and intra-band transitions between states and corresponding continuous light absorption across the solar spectrum. The combination of low reflection and high absorption, the lack of a distinct band gap, and a continuous DOS near and above E_F make $SrRuO_3$ an exciting light absorbing material.

2.2 Photovoltaic Devices and Response

We proceeded to study the potential of $SrRuO_3$-based heterostructures for solar applications by investigating the photoexcited carrier generation and transport in 100 nm TiO_2/ 50 and 10 nm $SrRuO_3$/ $SrTiO_3$ (001) Schottky junction photovoltaic devices. 100 nm thick, 100 μm diameter circular top contacts were created using the transparent conducting oxide 10% SnO_2-doped In_2O_3 (ITO) and the resulting devices were used to measure dark and light current-voltage (I-V) characteristics (**Figure 3**a). Light measurements were completed using a range of longpass glass filters in order to differentiate the photocurrent generated from light absorption in the $SrRuO_3$ alone as compared to that from the entire TiO_2/$SrRuO_3$ heterojunction. In all cases, AM1.5G light was used as the starting illumination and longpass glass filters cutting off progressively more of the AM1.5G spectrum at increasing wavelengths were used to step through the solar spectrum (details of all light-based measurements and additional information on the various longpass glass filters are provided (Supporting Information, Figure S2); throughout the remainder of the discussion we will refer to the filters by the longpass wavelength cutoff below which they have an optical density (OD) of 2 or higher [λ_{OD2}]).

Dark I-V measurements, here shown for a 100 nm TiO_2/ 10 nm $SrRuO_3$ heterostructure, reveal diode curves (black data, Figure 3a). Additional I-V studies as well as detailed views of the low-voltage response for both dark and light studies on

these devices are provided (Supporting Information, Figure S3). In all cases, the bias voltage for the I-V studies is applied to the top ITO contacts. Under AM1.5G light illumination, the diode curve is shifted in the positive current direction and a photovoltaic response is observed at zero applied voltage (Figure 3a). When the vast majority of light absorption in the TiO_2 is removed by utilizing longpass glass filters that cut-off light with energies larger than the band gap of TiO_2 (~3.4 eV for our films as measured via transmission-absorption which corresponds to all longpass glass filters with a $\lambda_{OD2} \geq 364$ nm), a series of diode curves with short circuit current densities (J_{SC}) of 2-10 μA/cm^2 are observed. The existence of a J_{SC} that is several orders-of-magnitude larger than the dark current even when illuminated by light with energies below the band gap of TiO_2 clearly demonstrates that the photocurrent is generated from light absorption in the $SrRuO_3$.

To glean further information about the nature of the photovoltaic behavior in the $TiO_2/SrRuO_3$ heterojunctions, we graph the J_{SC} observed as a function of the longpass glass filter λ_{OD2} for devices with both 10 and 50 nm of $SrRuO_3$ (Figure 3b). Again, the J_{SC} values are at least two orders-of-magnitude higher than the dark current (J_0). Recall that the $SrRuO_3$ has strong, continuous absorption across the entire energy range probed here whereas the TiO_2 only effectively absorbs light with energies above ~3.4 eV (Figure 3b). We also observe an exponential increase of the J_{SC} with decreasing cut-off wavelength which is a key to understanding the mechanism responsible for the visible light activity in these heterojunctions. The exponential dependence of the J_{SC} with λ_{OD2} suggests that fewer photoelectrons are transported over the Schottky barrier between the TiO_2 and $SrRuO_3$ as the longpass glass filters progressively remove more of the higher energy photons. It is obvious that the absorption of high-energy photons in the $SrRuO_3$ should result in the excitation of electrons to higher energy states thereby effectively increasing the probability that these excited electrons will have sufficient energy to overcome the Schottky barrier and be transported into the TiO_2. Additionally, it should be noted that the observed trends and values of the J_{SC} for heterojunctions based on both 10 nm and 50 nm $SrRuO_3$ films are essentially the same. This further supports the argument that the mechanism responsible for the observed photovoltaic effects is not bulk in nature, but arises from an effect near the $TiO_2/SrRuO_3$ interface since the 50 nm thick film should absorb ~3.8 times more light than the 10 nm thick film, but both exhibit similar J_{SC} values as a function of cut-off wavelength.

The driving force for this charge injection from the $SrRuO_3$ into the TiO_2 likely arises from the fact that there is a 6-to-7 order-of-magnitude difference in carrier concentration between TiO_2 and $SrRuO_3$ which results in the TiO_2 layer being fully depleted. Using standard equations, the depletion width of the TiO_2 can be calculated as $w \approx \sqrt{\frac{2\varepsilon_r\varepsilon_0}{q}\left(\frac{N_{TiO2}+N_{SRO}}{N_{TiO2}N_{SRO}}\right)\phi_b}$ where ε_r is the relative permittivity of anatase TiO_2 (39), ε_0 is the permittivity of free space, q is the charge of the carriers, N_{TiO2} is the carrier concentration of the TiO_2 (measured to be 10^{15}-10^{16} cm^{-3} for devices in this study), N_{SRO} is the carrier concentration of the $SrRuO_3$ (measured to be 8-9 × 10^{22} cm^{-3}), and ϕ_b is the Schottky barrier height between the materials (measured to be 1.3 V, details to be discussed later). Based on these numbers, the depletion width in the TiO_2 films is estimated to be between 620-1,990 nm. The thicknesses of TiO_2 layers used in this work are less than 100 nm and thus in all cases herein, the TiO_2 layers are expected to be fully depleted resuling in a built-in electric field that drives charge extraction from the $SrRuO_3$.

To better understand the operation of this device, we combined published values of work functions for these materials[30] and detailed electronic measurements to construct a proposed band diagram to help explain the observed photovoltaic response. The nature of the various electronic interfaces has been studied in detail. Using a sister device structure, ITO/TiO_2/0.5% Nb-doped $SrTiO_3$ (001), we were able to probe the nature of the ITO/TiO_2 interface. 0.5% Nb-doped $SrTiO_3$ (001) substrates are known to have metal-like conductivity, possess similar crystal structure and chemistry to $SrRuO_3$, and present a nearly invariant work function of 4.1 eV that allows for direct study of the electronic structure of the ITO/TiO_2 interface. Dark I-V studies and subsequent fitting of the positive-bias regime data with the Richardson-Nordheim equation reveal a Schottky barrier height of ~1.1 eV at the ITO/TiO_2 interface (Supporting Information, Figure S4a). A band diagram for the ITO/TiO_2/0.5% Nb-doped $SrTiO_3$ (001) device structure is also provided (Figure S4b). Armed with this information about the ITO/TiO_2 interface, we proceeded to analyze the ITO/TiO_2/$SrRuO_3$ heterojunctions. Using a similar process and fitting the positive-bias regime of the dark I-V studies of these devices, we extracted a Schottky barrier height at the $TiO_2/SrRuO_3$ interface of ~1.3 eV. A proposed dark, un-biased band diagram for the ITO/TiO_2/$SrRuO_3$ heterojunction is provided (Figure 3c). Thus the operation of the photovoltaic devices is likely influenced by two major factors. First, the large difference in carrier concentration between the TiO_2 and $SrRuO_3$ results in full depletion of the TiO_2 layer and formation of a built-in field that could help extract photo-excited hot-carriers from the $SrRuO_3$. Second, the small difference in the Schottky barrier heights at the two interfaces (i.e., ITO/TiO_2 and $TiO_2/SrRuO_3$) further supports the formation of a net (small) electric field in the TiO_2 that favors the separation and transport of photo-excited carriers. In comparison to previous studies of hot-carrier devices, in which photoelectrons were accepted by surface states on the TiO_2, in our system the carrier production and injection results from the unique electronic structure and resulting light absorption in the $SrRuO_3$ and the built-in electric field in the depleted TiO_2. This is the first observation and utilization of the strong light absorption of the "metallic" complex oxide $SrRuO_3$ and hot-carrier injection in this system in the context of an energy application.

2.3 Photocatalytic Devices and Response

To assess the photocatalytic performance of the $TiO_2/SrRuO_3$ heterojunctions we measured the photo-degradation of methylene blue (MB) dye. MB photo-degradation is a widely used method to evaluate the visible light activities of photocatalysts[31,32] and can be considered as a surrogate to photocatalytic water splitting when comparing one device to another. These studies were achieved using a collimated 300 W Xe arc lamp with an AM1.5G filter and condenser lens

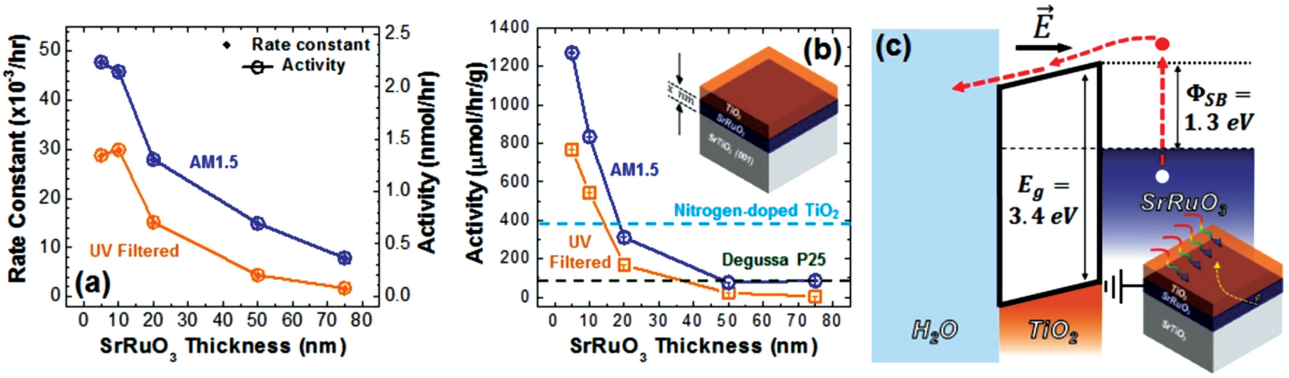

Figure 4. (a) Rate constant and activity and (b) mass-normalized photocatalytic activity of methylene blue photodegradation for 10 nm TiO_2/ x nm $SrRuO_3$ heterostructures. (c) Proposed band diagram of how hot-carrier injection gives rise to the photocatalytic response.

to produce 3,760 mW/cm^2 full AM1.5G spectrum light and 3,280 mW/cm^2 AM1.5G spectrum light filtered with a λ_{OD2} = 416 nm longpass glass filter (which removes more than 99.97% of light with energy above the ~3.4 eV band gap of TiO_2 and is henceforth referred to as UV-filtered light). Further details of the MB studies are provided (Supporting Information, Figure S5).

The photocatalytic activity of the heterostructures was studied as a function of the $SrRuO_3$ thickness and, for the range of thicknesses studied, the rate constant and initial reaction rate (activity) was observed to increase with decreasing film thickness under both AM1.5G illumination and UV-filtered light (**Figure 4**a) (the normalized MB concentration time trace data for all samples is provided (Supporting Information, Figure S6). To put this activity in context, we compare the performance of the $TiO_2/SrRuO_3$ heterostructures to that of a 10 nm $TiO_2/SrTiO_3$ control sample and the results of Ref. [32] which studied Degussa P25 and nitrogen-doped TiO_2 nano-powders under similar experimental conditions to those used here, i.e., high intensity light (390 nm laser light with a light intensity of 5,090 mW/cm^2), pH = 7 solution, and no electrolyte. We compared the mass-normalized activities (obtained by dividing by the total mass of the $TiO_2/SrRuO_3$ catalyst assuming the theoretical densities of 6.489 and 4.23 g/cm^3 for $SrRuO_3$ and TiO_2, respectively) and found that the normalized activity of the highest performing $TiO_2/SrRuO_3$ photocatalyst is more than 3 times higher than the equivalently normalized activity for nitrogen-doped TiO_2 and more than 25 times higher than the Degussa P25 nanopowders (despite our use of broad-band illumination with considerably less light intensity) (Figure 4b). Additionally, the $TiO_2/SrRuO_3$ heterojunction has 25 times higher mass-normalized activity than the 10 nm $TiO_2/SrTiO_3$ control sample. This enhanced performance is likely the result of the enhanced light absorption in the $SrRuO_3$ layer.

2.4 Thickness Dependence of Photocatalytic Response

To understand the increase in the photocatalytic activity with decreasing SrRuO--$_3$ film thickness, we explored a range of possible explanations including potential electronic, optical, and chemical changes which we will summarize here. For instance, based on our proposed model of hot-carrier injection, we explored whether multiple reflections of the incident light in an ultra-thin film could account for the strong thickness-dependent increase in the photocatalytic activity due to increased light absorption in the top several nanometers where there is an enhanced probability of such hot-carriers being injected. Based on the measured absorption coefficient of $SrRuO_3$ and the calculated reflectance values for the $TiO_2/SrRuO_3$ and $SrRuO_3/SrTiO_3$ interfaces we found that the amount of light absorbed in the top 2 nanometers of the $SrRuO_3$ could potentially be increased by ~40% when going from a 50 nm to 5 nm thick $SrRuO_3$ film. These calculations included up to 5 passes of the light through the thickness of the films after which the absorbed light intensity was <1% of the initial absorbed intensity. Although impressive, this does not account for the ~1650% increase in the mass normalized photocatalytic activity. Another possible explanation that was considered was that the surface potential (i.e., the reduction/oxidation potential) of the TiO_2 changes as a function of $SrRuO_3$ thickness. Although plausible, this is unexpected as all heterojunctions studied have TiO_2 films prepared in the same manner with the same phase (anatase), exposed surface facet ((001)), thickness (10 nm), effective defect density, and (as noted previously) all the TiO_2 films are uniformly depleted by the high carrier concentration of the underlying $SrRuO_3$ layer. Therefore the surface electrochemical properties of the TiO_2 films are expected to be the same for all heterojunction samples.

Additionally, we explored the evolution of the electronic transport of $SrRuO_3$ as a function of thickness. Using temperature- and magnetic field-dependent resistivity studies we were able to extract the resistivity, carrier density, and mobility for the $SrRuO_3$ films as a function of thickness and in $TiO_2/SrRuO_3$ heterojunctions. The room temperature resistivity (carrier concentration) for 50 nm and 10 nm $SrRuO_3$ films were found to 227 μΩ-cm (8.43×10^{22} cm^{-3}) and 281 μΩ-cm (8.93×10^{22} cm^{-3}), respectively. Even subsequent growth of a 10 nm TiO_2 layer on the $SrRuO_3$ film had little effect on the room temperature resistivity and carrier concentrations (267 μΩ-cm and 9.02×10^{22} cm^{-3}, respectively). In all cases the room-temperature carrier mobility was found to be between 0.19-0.25 cm^2 V^{-1} s^{-1}. These values are consistent with that expected for $SrRuO_3$

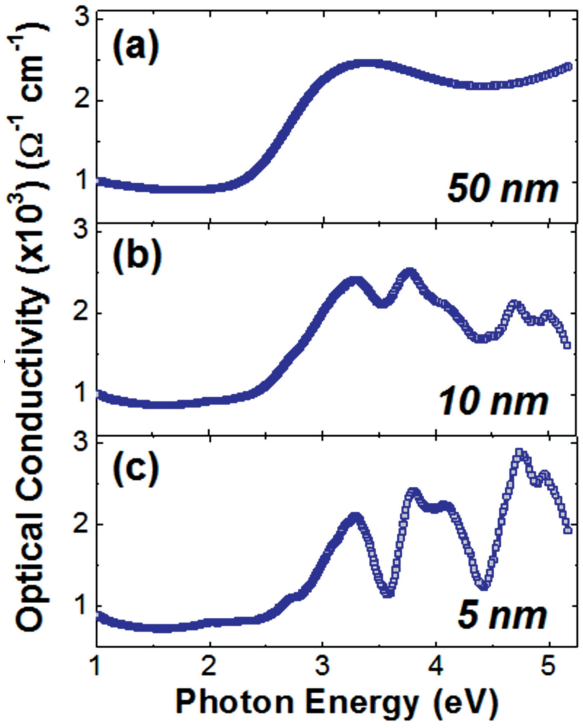

Figure 5. (a), (b), and (c) Optical conductivity of 50, 10, and 5 nm thick $SrRuO_3$ thin films, respectively.

films from the extensive literature[19] and with prior thickness dependent studies[33–35] which suggest a critical thickness for changes in the near E_F electronic structure (and deviation from the expected metallic and magnetic properties) of 4-5 monolayers (~1.5-2 nm) and relatively little effect on those properties within the range of thicknesses studied herein (5-50 nm).

Such transport studies probe the near and below E_F electronic structure of materials, but the process of photo-excitation generates electrons at higher energy states which cannot be probed with these techniques. In the context of our proposed mechanism of hot-carrier injection, it is important not only to understand the near- and below-E_F response of the material, but also the above E_F opto-electronic response of the material as a function of thickness. To do this, we utilized optical conductivity which is a powerful tool for studying above-E_F electronic states in materials[36] and can be correlated to the band structure in that it provides a quantitative measurement of the probability of optical transitions convoluted with the electronic DOS.[37–39] According to Fermi's golden rule, the optical transition rate from an initial state to a final state is a function of the DOS of the initial and final states. For solids, the transition matrix element that describes the nature of this transition also depends on the overlap integral between the initial and final states. In $SrRuO_3$ the O 2*p* bands are hybridized with the Ru 4*d* and the Sr 4*d* bands resulting in a complex DOS.[40,41] Researchers have identified a number of possible transitions in this system including transitions from the O 2*p* to the Ru t_{2g} and e_g and the Sr 4*d* states and additional inter- and intra-atomic transitions (which are possible due to the hybridization with the O 2*p* bands and/or local distortions)[36] that include transitions from the occupied Ru t_{2g} states to the unoccupied Ru t_{2g} and e_g and the Sr 4*d* states.[26]

The optical conductivity, σ, was calculated from the measured n and k values as $\sigma = nk\omega/2\pi$. Our measurements of the optical conductivity of thick $SrRuO_3$ films (>25 nm) (**Figure 5**a) are consistent with previous reports[26,42] which reveal a lower optical conductivity to the high-energy side of the Drude peak (not shown in Figure 5) and smooth, undulating features at photon energies greater than ~2.5 eV. Dramatic differences, however, are observed in thinner films where there is a clear evolution of fine structure and distinct separation of states in the $SrRuO_3$ optical conductivity spectra (Figure 5b, c). Although the electronic DOS well above E_F has only been studied in bulk-like films and samples (not ultra-thin films), the evolution of sharp features in the DOS is observed across a range of energies in first-principles calculations for ultra-thin $SrRuO_3$.[34] We propose that the observed changes in the optical conductivity are indicative of changes in the electronic structure as noted in the literature[43] and that this change in electronic structure could also produce changes in the excited (above E_F) electron dynamics thereby impacting the hot-carriers. To prove such a connection, additional studies of excited carrier dynamics (i.e., transient carrier lifetimes) should be completed. Such experiments, however, are expected to be difficult due to the potentially extremely short lifetimes of these excited carriers and the relatively high energy of photons needed to probe the features in the optical conductivity and are beyond the scope of this treatment.

3. Conclusion

In conclusion, we observe that the "metallic" oxide $SrRuO_3$ possesses a high absorption coefficient (> 1.5×10^5 cm^{-1}) and low reflectance (< 25%) over the entire visible light spectrum due in part to a complex DOS and a nearly continuous range of inter- and intraband excitations that are possible in the material. From light-dark I-V studies, we observe evidence for photon-excited hot-carrier generation and injection from $SrRuO_3$ to TiO_2. The strong light absorption in $SrRuO_3$ can, in turn, be used to increase the efficiency of TiO_2 as a photovoltaic and photocatalytic material. These novel optical properties and the resulting high photoelectrochemical performance of the TiO_2/$SrRuO_3$ heterostructures provide an interesting new approach that could advance the field of photocatalysis and further broaden the potential applications of other metallic oxides.

4. Experimental Section

Synthesis of materials: Films were grown using pulsed-laser deposition. Thin films of $SrRuO_3$ were grown at a laser fluence of 1.05 J/cm^2 and laser repetition rate of 5 Hz at 660 °C in 100 mTorr of oxygen. Following growth of single-layer $SrRuO_3$ films, the samples were cooled to room temperature in 760 Torr of oxygen. Thicknesses were measured *ex situ* via fitting of X-ray diffraction Kiessig fringes and X-ray reflectivity studies. For TiO_2/$SrRuO_3$ heterostructures, following the growth of the $SrRuO_3$ layer, the sample was cooled *in situ* to 600°C where the TiO_2 layers were deposited at a laser fluence of 0.96 J/cm^2 and laser repetition rate of 10 Hz in 1 mTorr of oxygen. Following the growth, the films were cooled to room temperature in 1 mTorr of oxygen. All films

were examined following growth via X-ray diffraction and atomic force microscopy. All films studied were single-phase, fully epitaxial anatase TiO_2 (00*l*-oriented) with root-mean-square surface roughness < 0.5 nm regardless of the $SrRuO_3$ thickness. The transparent conducting oxide used in this study was 10% SnO_2-doped In_2O_3 (ITO). 100 nm thick ITO thin films were deposited through photolithography-defined photoresist masks at a laser fluence of 1.0 J/cm^2 and laser repetition rate of 5 Hz at room temperature in 20 mTorr of oxygen. Following growth and removal of photo-resist, samples were annealed at 300°C for 30 minutes and subsequently cooled to room temperature at 20 mTorr to improve electronic and optical properties of the ITO.

Supporting Information

Supporting Information is available from the Wiley Online Library or from the author.

Acknowledgements

S. Lee and B. A. Apgar contributed equally to this work. Work on photovoltaic and photocatalytic response was supported by the International Institute for Carbon-Neutral Energy Research (WPI-I2CNER), sponsored by the Japanese Ministry of Education, Culture, Sport, Science and Technology. Optimization of $SrRuO_3$ growth and characterization of $SrRuO_3$ optical properties was partially supported by the U.S. Department of Energy under grant DEFG02-07ER46459. Experiments were carried out in part in the Materials Research Laboratory Central Facilities. The authors thank E. Breckenfeld, N. Bronn, and Julio Soares for fruitful discussions related to electronic transport and light absorption studies.

Received: December 28, 2012
Revised: February 4, 2013
Published online: April 25, 2013

[1] A. Fujishima, X. T. Zhang, D. A. Tryk, *Surf. Sci. Rep.* **2008**, *63*, 515.
[2] F. E. Osterloh, *Chem. Mater.* **2008**, *20*, 35.
[3] B. Oregan, M. A. Gratzel, *Nature* **1991**, *353*, 737.
[4] G. K. Mor, O. K. Varghese, M. Paulose, K. Shankar, C. A. Grimes, *Sol. Energ. Mat. Sol. C* **2006**, *90*, 2011.
[5] W. Choi, A. Termin, M. R. Hoffmann, *J. Phys. Chem.* **1994**, *98*, 13669.
[6] A. Zaleska, *Rec. Patents Eng.* **2008**, *2*, 157.
[7] R. Asahi, T. Morikawa, T. Ohwaki, K. Aoki, Y. Taga, *Science* **2001**, *293*, 269.
[8] A. J. Nozik, *Appl. Phys. Lett.* **1977**, *30*, 567.
[9] N. Serpone, E. Borgarello, M. Grätzel, *J. Chem. Soc. Chem. Commun.* **1984**, 342.
[10] K. Vinodgopal, I. Bedja, P. V. Kamat, *Chem. Mater.* **1996**, *8*, 2180.
[11] M. Ocana, W. P. Hsu, E. Matijevic, *Langmuir* **1991**, *7*, 2911.
[12] M. G. Walter, E. L. Warren, J. R. McKone, S. W. Boettcher, Q. Mi, E. A. Santori, N. S. Lewis, *Chem. Rev.* **2010**, *110*, 6446.
[13] A. J. Nozik, R. Memming, *J. Phys. Chem.* **1996**, *100*, 13061.
[14] A. J. Nozik, *Physica E* **2002**, *14*, 115.
[15] W. A. Tisdale, K. J. Williams, B. A. Timp, D. J. Norris, E. S. Aydil, X.-Y. Zhu, *Science* **2010**, *328*, 1543.
[16] J. B. Sambur, T. Novet, B. A. Parkinson, *Science* **2010**, *330*, 63.
[17] J. A. Turner, A. J. Nozik, *Appl. Phys. Lett.* **1982**, *41*, 101.
[18] M. A. Fox, M. T. Dulay, *Chem. Rev.* **1993**, *92*, 341.
[19] G. Koster, L. Klein, W. Siemons, G. Rijnders, J. S. Dodge, C.-B. Eom, D. H. A. Blank, M. R. Beasley, *Rev. Mod. Phys.* **2012**, *84*, 253.
[20] A. D. Rakic, *Appl. Opt.* **1995**, *34*, 4755.
[21] E. D. Palik, *Handbook of Optical Constants of Solids*, Academic Press, Boston, MA, USA **1985**.
[22] C. L. Chen, Y. Cao, Z. J. Huang, Q. D. Jiang, Z. Zhang, *Appl. Phys. Lett.* **1997**, *71*, 1047.
[23] P. B. Allen, H. Berger, O. Chauvet, L. Forro, T. Jarlborg, A. Junod, B. Revaz, G. Santi, *Phys. Rev. B* **1996**, *53*, 4393.
[24] K. Fujioka, J. Okamoto, T. Mizokawa, A. Fujimori, I. Hase, M. Abbate, H. J. Lin, C. T. Chen, Y. Takeda, M. Takano, *Phys. Rev. B* **1997**, *56*, 6380.
[25] J. Okamoto, T. Mizokawa, A. Fujimori, I. Hase, M. Nohara, H. Takagi, Y. Takeda, M. Takano, *Phys. Rev. B* **1999**, *60*, 2281.
[26] J. S. Lee, Y. S. Lee, T. W. Noh, K. Char, J. Park, S.-J. Oh, J.-H. Park, C. B. Eom, T. Takeda, R. Kanno, *Phys. Rev B* **2001**, *64*, 245107.
[27] K. Maiti, R. S. Singh, *Phys. Rev. B* **2005**, *71*, 161102.
[28] J. M. Rondinelli, N. M. Caffrey, S. Sanvito, N. A. Spaldin, *Phys. Rev. B* **2008**, *78*, 155107.
[29] A. Georges, G. Koltiar, W. Krauth, M. J. Rezenberg, *Rev. Mod. Phys.* **1996**, *68*, 13.
[30] M. Minohara, I. Ohkubo, H. Kumigashira, M. Oshima, *Appl. Phys. Lett.* **2007**, *90*, 132123.
[31] R. W. Matthews, *Water Res.* **1991**, *25*, 1169.
[32] J. L. Gole, J. D. Stout, C. Burda, Y. Lou, X. Chen, *J. Phys. Chem. B* **2004**, *108*, 1230.
[33] D. Toyota, I. Ohkubo, H. Kumigashira, M. Oshima, T. Ohnishi, M. Lippmaa, M. Takizawa, A. Fujimori, K. Ono, M. Kawasaki, H. Koinuma, *Appl. Phys. Lett.* **2005**, *87*, 162508.
[34] Y. J. Chang, C. H. Kim, S.-H. Phark, Y. S. Kim, J. Yu, T. W. Noh, *Phys. Rev. Lett.* **2009**, *103*, 057201.
[35] J. Xia, W. Siemons, G. Koster, M. R. Beasley, A. Kapitulnik, *Phys. Rev. B* **2009**, *79*, 140407.
[36] J. H. Jung, K. H. Kim, D. J. Eom, T. W. Noh, E. J. Choi, J. Yu, Y. S. Kwon, Y. Chung, *Phys. Rev. B* **1997**, *55*, 15489.
[37] P. Y. Yu, M. Cardona, *Fundamentals of Semiconductors: Physics and Materials Properties*, Springer, New York, NY, USA **2005**.
[38] G. Dresselhaus, M. S. Dresselhaus, *Optical Properties of Solids*, Ed. J. Tauc, Academic Press, New York, NY USA **1966**.
[39] A. J. Millis, *Optical Conductivity and Correlated Electron Physics* in *Strong Interactions in Low Deminsions*, Ed. D. Baeriswyl, L. Degiorgi, Springer-Verlag, Berlin, **2004**.
[40] J. Park, S.-J. Oh, J.-H. Park, D. M. Kim, C.-B. Eom, *Phys. Rev. B* **2004**, *69*, 085108.
[41] J. Kim, J. Chung, S.-J. Oh, *Phys. Rev. B* **2005**, *71*, 121406.
[42] K. W. Kim, J. S. Lee, T. W. Noh, S. R. Lee, K. Char, *Phys. Rev. B* **2005**, *71*, 125104.
[43] M.-R. Li, J. P. Carbotte, *Phys. Rev. B* **2002**, *66*, 155114.